JANUARY SIMULATION OF CLOUDS WITH A PROGNOSTIC CLOUD COVER SCHEME

E. Roeckner and U. Schlese

Meteorologisches Institut der
Universität Hamburg, F.R.G.

Abstract

Based on the work of Sundqvist (1978), a cloud prediction scheme has been developed and tested interactively with radiation in a series of January GCM-simulations. The cloud liquid water content (LWC) is calculated by numerical integration of the LWC continuity equation with sources (condensation) and sinks (evaporation, precipitation). Precipitating water is allowed to evaporate in non-saturated sub-cloud layers. The scheme allows for fractional cloudiness (horizontally). Cloud-cover and LWC determine the radiative properties of the model clouds.

The zonally averaged short- and longwave radiation budget at the top of the atmosphere and at the earth's surface are simulated mostly within the range of observational errors. Larger differences are found in the tropical net solar radiation budget at the surface caused by a significantly underestimated low-level cloud amount (<10%) at those latitudes. On the other hand, at high latitudes (north of 50°N) low-level cloudiness (up to 60% in the zonal mean) is significantly overestimated. Both errors are related to the inadequately parameterized conversion rate(cloud droplets ⟶ rain drops) which turned out to be the most sensitive process in the present scheme and which will have to be improved in the future. Surprisingly, advection and turbulent diffusion of cloud LWC are of secondary importance only.

A major advantage of the scheme is that it produces a reasonable distribution of cloud LWC which is probably due to the inclusion of the clouds in the hydrological cycle of the model.

1. INTRODUCTION

Due to theoretical and observational limitations, the representation of clouds in weather prediction models and GCM's is still in the experimental stage. This is true not only for cloud cover but even more for the liquid water content (LWC) in the clouds. Both parameters, among others, significantly affect the radiation budget of the atmosphere and of the surface. They should therefore be carefully treated in models for which cloud-radiation interactions are important.

In most models, however, the radiative properties of clouds (reflectivity, absorbtivity and transmissivity) are prescribed. Only two attempts, to our knowledge, have been made at calculating the radiative fluxes from the LWC of the clouds (Geleyn, 1981; Hense and Heise, 1984). In both methods the LWC is parameterized in terms of large-scale variables (saturation water vapour mixing ratio and spatial variance of vertical velocity, respectively).

In this paper we will report on experiments we have made with a cloud prediction scheme that is based largely on the proposal of Sundqvist (1978) of calculating cloud amount and LWC from the governing equations, including the LWC continuity equation. The scheme is being tested interactively with radiation (Hense et al., 1982) in the Hamburg University GCM (Roeckner, 1979). The method is outlined in Section 2. Results from January simulations are given in Section 3.

2. THE METHOD

2.1 Governing equations

The equations relevant for the discussion of the cloud prediction scheme are those for the mixing ratios of water vapour (q) and cloud liquid water (m), and the thermodynamic equation which may be written in a symbolic as

$$\frac{\partial q}{\partial t} = Adv(q) + Dif(q) + Con(q) - C + E \quad (1)$$

$$\frac{\partial m}{\partial t} = Adv(m) + Dif(m) + C - P \quad (2)$$

$$\frac{\partial T}{\partial t} = Adv(T) + Dif(T) + Con(T) + Rad + L/c_p(C - E) \quad (3)$$

where Adv, Dif, Con, Rad denote the respective changes due to advection, turbulent diffusion, moist and dry convection, and radiation. The cloud microphysical terms are denoted by

C Condensation of water vapour if $q > q_s$ $(C > 0)$ or
Evaporation of cloud liquid water m if $q < q_s$ and $m > 0$ $(C < 0)$,

P Rate of precipitation formation due to coalescence processes,

E Evaporation rate of precipitating water in non-saturated layers.

At present we consider transitions between the liquid and the gaseous phase only.

The solution of the system (1) - (3), together with the momentum equations which have been omitted for convenience, is complicated by the fact that clouds (not only cumulus clouds but also stratiform clouds) are often observed to form in a non-saturated environment, depending on the intensity of small-scale processes. Therefore, in large-scale models one should allow for the occurrence of subgrid-scale condensation, i.e. fractional cloud cover.

2.2 Fractional cloud cover

Following Sundqvist (1978), we assume that if the relative humidity r in a grid volume exceeds a threshold value $r_o < 1$ (which has to be specified or parameterized) a layer cloud will form with fractional cover $b > 0$, but filling the whole depth of the respective model layer. In this case, the solution of the system (1) - (3) is achieved by solving the equations separately for the cloudy part b and the cloud-free part (1-b) for a unit area.

The equations (1)-(3) may then be written according to

$$\frac{\partial \hat{q}}{\partial t} = \hat{R}_q - \hat{C} + \hat{E} \tag{4}$$

$$\frac{\partial \hat{m}}{\partial t} = \hat{R}_m + \hat{C} - \hat{P} \tag{5}$$

$$\frac{\partial \hat{T}}{\partial t} = \hat{R}_T + L/c_p \, (\hat{C} - \hat{E}) \tag{6}$$

where the "R"-terms include all changes due to advection, diffusion etc. of the respective variables and (^) denotes a weighted average of the respective term in the cloudy (b)-part $(\,)^+$ and in the cloud-free (1-b)-part $(\,)^-$ according to

$$\hat{X} = bX^+ + (1-b)X^- \tag{7}$$

For closing the system (4)-(6) the separation (7) is done, however, only for the "moist" terms, i.e. for the set X = (q,m,C,E,P), so that we have

$$\hat{X} = b\hat{X} + (1-b)\hat{X} \qquad \text{for } X = (T, R_q, R_m, R_T) \tag{8}$$

Furthermore, no interaction is allowed between the cloudy and the cloud-free parts. For solving the system (4)-(6), together with the definitions (7) and (8), we have to specify X^+ and X^- for X = (q,m). A natural choice is (cf. Sundqvist,1978)

$$q^+ = q_s \; ; \quad q^- = q_o = q_s r_o \; ; \quad m^- = 0 \tag{9}$$

so that from (7) we have

$$\hat{q} = b\hat{q}_s + (1-b)\hat{q}_s r_o \qquad \text{with } \hat{q}_s = q_s\,(\hat{T}) \tag{10}$$

$$\hat{m} = bm^+ \tag{11}$$

According to (10) the fractional cloud cover is defined to be

$$b = \frac{\hat{q} - q_o}{\hat{q}_s - q_o} = \frac{\hat{r} - r_o}{1 - r_o} \tag{12}$$

which is used to define the liquid water mixing ratio m^+ in (11). Thus, according to (7)-(12), all subgrid-scale variables $(\ )^+$ and $(\ )^-$ can be traced back to large-scale variables $(\hat{\ })$. The only free parameter introduced so far is the threshold relative humidity r_o.

The solution method will be demonstrated by looking at the moisture equation (4) only. Inserting the time derivative of (10) into (4) yields together with (7) and (8)

$$\frac{\partial \hat{q}}{\partial t} = b\frac{\partial \hat{q}_s}{\partial t} + (1-b)\frac{\partial q_o}{\partial t} + (\hat{q}_s - q_o)\frac{\partial b}{\partial t}$$

$$= b(\hat{R}_q - C^+ + E^+) + (1-b)\cdot(\hat{R}_q - C^- + E^-) \qquad (13)$$

Thus, the mean change $\frac{\partial \hat{q}}{\partial t}$ is composed of three terms representing the condensation (evaporation) rate in the cloudy part, the change of moisture in the cloud-free part and the cloud-cover change, respectively. Since the actual partitioning of these three contributions is unknown we have to set up some plausible arrangement. At present, we assume (cf. Sundqvist,1978) that a moisture supply $(\hat{R}_q > 0)$, for example, is distributed among two terms only, i.e. the condensation rate in the b-part and the cloud-cover change by the moisture supply in the (1-b)-part. The solution is achieved in two steps (in order to avoid solving a prognostic equation for b).

Step 1: $\frac{\partial b}{\partial t} = 0$ (preliminary)

In this case the b-terms and (1-b)-terms in (13) may be combined into two symmetric equations that formally represent the situations that occur in standard condensation schemes, i.e. a moisture change in unsaturated air and condensation in saturated air (if $\hat{R}_q > 0$)

$$\frac{\partial q_o}{\partial t} = \hat{R}_q - C^- + E^- \qquad \text{(cloud-free part)} \qquad (14)$$

$$\frac{\partial q_s}{\partial t} = \hat{R}_q - C^+ + E^+ \qquad \text{(cloudy part)} \qquad (15)$$

for $b > 0$, i.e. for $\hat{q} > q_o$.

Analogous equations are obtained for the liquid water mixing ratio m. Solving (14), (15) together with the remaining equations at a time-step (n) and weighting the solutions with (1-b) and (b), respectively, then according to (13) we obtain the solution for the mean $\frac{\partial \hat{q}}{\partial t}^{(n)}$ so that the "new" moisture $\hat{q}^{(n+1)}$ is known.

Step 2: According to (12) the cloud-cover is related to the mean moisture (and temperature) so that after Step 1 we obtain

$$b^{(n+1)} = \frac{\hat{q}^{(n+1)} - q_o^{(n+1)}}{\hat{q}_s^{(n+1)} - q_o^{(n+1)}} = \frac{\hat{f}^{(n+1)} - r_o}{1 - r_o} \qquad (16)$$

which includes the assumption that the relative humidity in the cloud-free part r_o remains unchanged so that the total moisture supply in (1-b) is used for the formation of new clouds.

Though the solution method outlined above is different from that of Sundqvist(1978), the results should be similar because the basic assumptions are identical.

2.3 Cloud microphysical processes

As in most standard condensation schemes a threshold relative humidity of 100% is used. However, this applies for the cloudy part of a grid-volume (cf. equ. (15)) so that subgrid-scale condensation is allowed if the mean relative humidity $\hat{f}$ exceeds a threshold value $r_o < 1$ (cf.section 2.2).

The parameterization of precipitation formation has to take into account the growth of cloud droplets to raindrops by condensation and coalescence processes. Following a proposal of Sundqvist(1978), the intensity of raindrop production has been related to liquid water content according to

$$P = C_o(1 - \exp-(m/m_r)^2) \cdot m \qquad (17)$$

where C_o^{-1} is the e-folding time for the decrease of cloud liquid water by precipitation in the limit $m \gg m_r$. For $m \ll m_r$ clouds are essentially in the non-precipitating stage so that $m = m_r$ approximately defines the limit between the non-precipitating clouds and those that are in a mature precipitating stage.

Evaporation of rainwater is parameterized according to Kessler(1969) from the assumption of a Marshall-Palmer raindrop spectrum resulting in

$$E \sim -(q - q_s) \cdot (Pr)^{1/2} \qquad (18)$$

where $(q-q_s)$ represents the saturation deficit and Pr the precipitation rate at the respective level. According to (18) evaporation of rainwater is allowed only in the cloud-free part of a grid-volume so that E^+ in (15) vanishes.

2.4 Choice of constants

The present scheme contains three free constants, namely r_o, C_o and m_r. The threshold relative humidity r_o should depend on the grid-size and on the intensity of subgrid-scale processes. A reduction of r_o tends to increase the probability of cloud formation but decreases the mean relative humidity in the grid volume by increased precipitation which in turn decreases the probability of cloud formation. This kind of negative feedback reduces the sensitivity of r_o as compared to standard relative humidity schemes where the clouds are not allowed to interact with the hydrological cycle. However, the present scheme is sensitive to the choice of the

"precipitation parameters" C_o and m_r that govern not only the liquid water in the clouds but also the cloud-cover distribution.

In the experiments discussed in section 3 we used the following values that were derived from a number of sensitivity studies with a coarse-grid GCM:

$$r_o = \begin{cases} 0.8 & \text{for non-convective situations} \\ 0.6 & \text{for convective situations} \end{cases} \tag{19}$$

$$C_o = 5 \cdot 10^{-4} \ s^{-1} \tag{20}$$

$$m_r = \begin{cases} 0.001 \ g/kg & \text{for high clouds} \\ 0.1 \quad " \quad " & \text{middle and low clouds} \end{cases} \tag{21}$$

The coice of (almost) uniform constants for all types of clouds is an over-simplification which will lead to substantial errors as will be obvious from the results presented in section 3. Therefore, the precipitation process is at present being modified so as to allow for the accelerated ice-crystal growth in a temperature range between approximately $-10^{\circ}C$ and $-20^{\circ}C$ ("Bergeron process").

2.5 Convective clouds

The present scheme does not include the explicit representation of convective cloud-cover. This might be tolerable because active cumulus clouds are known to cover just a few percent of the large-scale environment. However, cumulus clouds modify their environment not only by heating but they also detrain moisture which may lead to the formation of stratiform clouds covering a much larger fractional area than the active cumulus cells. These stratiform clouds being a byproduct of cumulus convection are included in the present scheme by simply increasing the probability of cloud formation in convective situations (19). They interact with the cumulus clouds indirectly by modification of the radiation field.

2.6 Advection and diffusion

From sensitivity tests with a coarse-grid GCM we may conclude that advection and turbulent diffusion are the smallest terms in the LWC continuity equation (2) and can therefore be safely neglected. This unexpected result may be understood from the fact that the liquid portion in the clouds is generally two or more orders of magnitude smaller than the vapour content. The dominating LWC production term is the condensation of water vapour which is comparable in magnitude to the water vapour advection term and hence at least two orders of magnitude larger than the LWC advection term. This is also true for the dissipation term P in (2) so that the LWC time rate of change is governed by the source and sink terms only which depend, however, crucially on the advection of water vapour and potential temperature.

The results presented in section 3 have been obtained, however, with the complete scheme.

3. GCM SIMULATIONS

3.1 The model

The cloud scheme described in section 2 has been tested in the Hamburg University model (Roeckner,1979). The model covers the Northern Hemisphere with a resolution of 2.8125° and 3 $\Delta\sigma$-layers with the top at 100mb. Tendency smoothing of all prognostic variables polewards of 50°N permits a time-step (leap-frog) of 4 min. A non-linear fourth-order horizontal diffusion scheme is applied to potential temperature and to the mixing ratios of water vapour and cloud liquid water. Additionally, mean sea level pressure and momentum are smoothed with a numerical filter at irregular intervals (3-6 hours) depending on the small-scale noise production of the model.

For moist convection we use the Kuo-scheme with a relative humidity depen-

dent partitioning between convective heating and moistening. The surface fluxes are calculated from a generalized similarity theory for the whole boundary layer. The radiation model has been adopted from Hense et al. (1982). It uses a two-stream approximation with six spectral intervals in the thermal and four in the solar region. The fluxes are calculated interactively with the GCM which provides temperature, cloud-cover and the mixing ratios of water vapour and cloud liquid water. The concentrations of ozone, aerosols and CO_2 are prescribed. Different aerosol distributions are used in rural, maritime and polar regions and on high terrain.
The vertical resolution of the radiation model differs from that of the GCM: The troposphere is resolved by 6 layers. The temperature at the top of the stratosphere which is dynamically inactive in our model has been prescribed by zonally averaged climatological values. Clouds are allowed to form only in the upper part of each GCM-layer, i.e. at heights of approximately (100-250mb), (400-550mb) and (700-850mb), respectively. Cloud overlap is assumed to be random. Finally, the cloud- and condensation model used is that discussed in section 2.

3.2 The experiments

The model was integrated up to 150 days in the perpetual January mode, including the diurnal cycle. Realistic surface boundary data have been used, i.e. grid-area averaged orography, surface roughness length depending on subgrid-scale orography, and climatological distributions of sea surface temperature, soil moisture and albedo. Initial conditions are from 2 January 1974.
A series of 60d-experiments has been performed with a coarse-grid version of the model (11.25^{o}), in order to study the parameter sensitivity of the cloud scheme and, moreover, to compare it with a diagnostic relative humidity scheme (Geleyn, 1981). The bulk of the results shown in the next

section has been obtained, however, from the first 30d of the integration with the 2.8°-grid version.

3.3 Results

Two problems arise when the performance of a cloud scheme is examined in GCM simulations. Firstly, the simulated cloud distributions depend largely on the characteristics of the model (structure, dynamics, parameterizations) so that errors in the model climate will also be reflected in the cloud amount. Secondly, the currently available cloud climatologies differ considerably. Satellite-based observations of radiation parameter may be used additionally; however, the radiation budget is not only affected by clouds but also by temperature and various absorbers other than clouds, e.g. water vapour. Having all this in mind, we will not be able in this section to assess the performance of our cloud scheme in a completely satisfying way. However, a few indications at least can safely be given.

Time series of grid-point values

Before comparing simulations and observations it seems to be useful to look at some properties of the scheme and to compare it with a standard relative humidity scheme. Figure 1 shows a comparison of the present scheme (upper panel) with a "diagnostic" scheme (Geleyn,1981) where cloud-cover is related to relative humidity in a quadratic relationship and cloud LWC is assumed to be a constant fraction (0.2%) of the saturation water vapour mixing ratio. The short period fluctuations in the cloud parameters are caused by the diurnal cycle with large (small) values during the night (daytime). Disregarding the time-mean values of r,b and LWC which depend largely on the free parameter of the schemes, the time variations (being almost independent on parameter choice) are significantly different in both schemes: The prognostic scheme shows a high degree of coherence

between the large-scale forcing (r) and the clouds. This should be expected because the dominating source term for both, b and LWC, is the condensation rate. On the other hand, in the diagnostic scheme the cloud cover b depends also on relative humidity; however, the LWC is independently calculated from temperature alone.

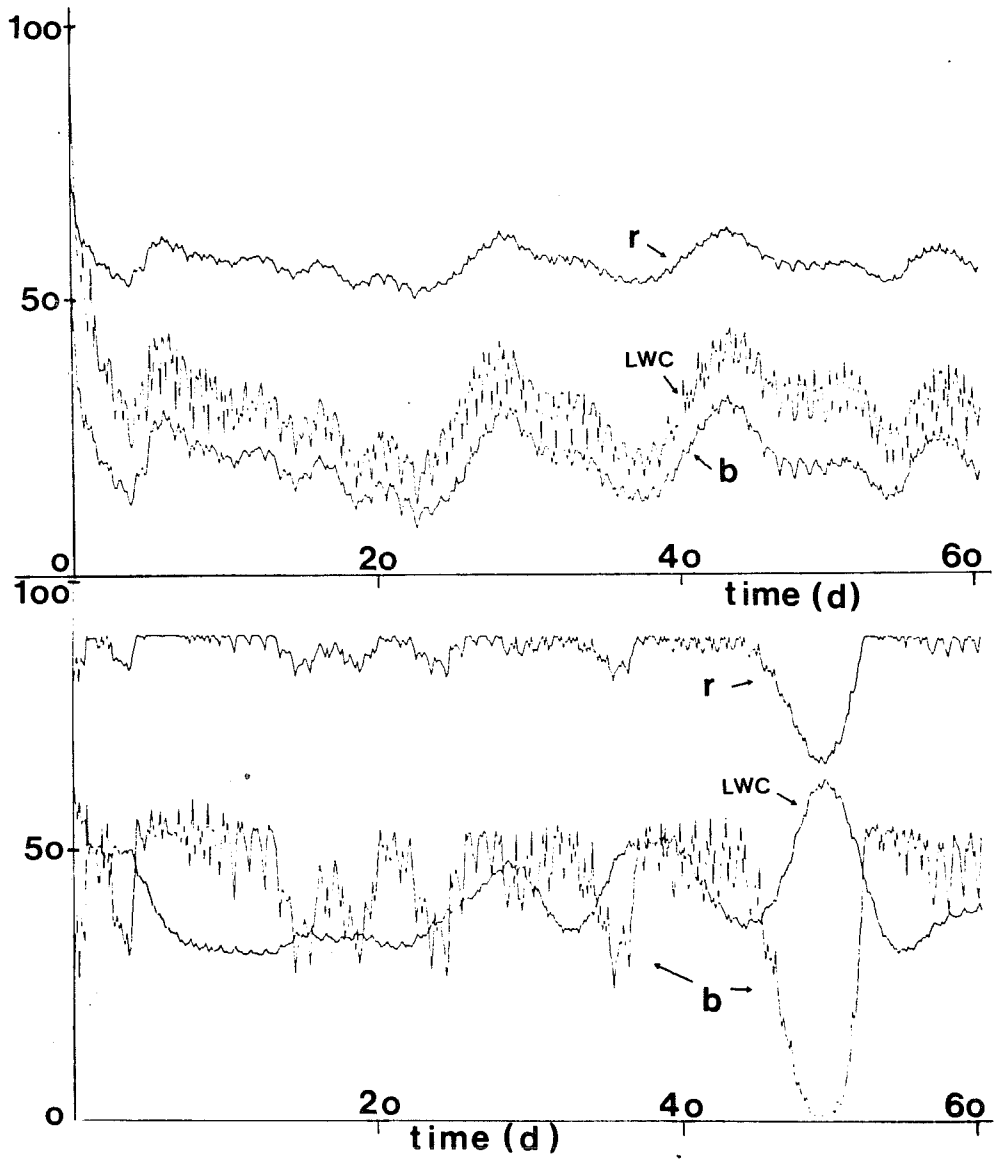

Fig.1 Time series of 850mb relative humidity (r), cloud-cover (b) and liquid water content (LWC) at a grid-point in the sub-tropical North Atlantic (46°W, 34°N) for two cloud schemes.
Upper panel: "Prognostic" scheme (based on LWC equation)
Lower panel: "Diagnostic" scheme (Geleyn,1981)
Units: % for r,b and g/m^2 for LWC
The temporal resolution of the time series is 3 hours.

This explains the fact that b and LWC in the diagnostic scheme tend to be out of phase which is striking around day 50: The relative humidity drop caused by potential temperature advection results in a rapid decrease of cloud cover (which is realistic) but in an increase of LWC (which is unrealistic). A further difference is that the diagnostic scheme reveals larger short-period fluctuations in b which can be understood from the following facts: The relationship between b and r is linear in the prognostic scheme but quadratic in the diagnostic one. Moreover, changes in the source term by water vapour advection are distributed among both cloud parameters, b and LWC, in the prognostic scheme (cf. equ.(13)) which results in a damping of the b-fluctuations as compared to the diagnostic scheme.

Hemispheric averages

From table 1 showing simulated and observed cloud, and radiation parameters for January averaged over the Northern Hemisphere we get a first insight into the "global" performance of the cloud scheme. Obviously, the correspondence is quite encouraging. One should note, however, that the observed cloud cover is an objective estimate for January 1977 only and that there are other climatologies that differ considerably from that of Gordon et al.(1984).

Furthermore, from table 1 we see that there seems to be no significant trend in the 150d-integration: The mean over the first month (0-30d) is close to the mean over the whole period. In order to minimize errors that might possibly be introduced by the "climate drift" of the model, we shall in the following concentrate on the first month when the simulated mass and wind fields are not too far away from climatology as will be shown later.

Parameter	Units	Exp(0-30d)	Exp(0-150d)	Obs	(Source)
Clouds					
High	%	22.5	24.7	21.8	Gordon et al.(1984)
Middle	%	11.5	12.0	19.6	"
Low	%	27.4	27.6	24.9	"
Total	%	45.1	46.2	50.3	"
LWC	g/m^2	57.7	55.3	-	
Radiation (Top)					
Albedo	%	28.9	29.0	29.0	Stephens et al. (1981)
F(up)	W/m^2	220.	219.	222.	
R(net)	"	-59.0	-57.4	-60.2	"
Radiation (Surface)					
F(net)	"	-68.1	-69.1	-72.4	Schutz and Gates (1971)
S(net)	"	118.	117.	124.	
R(net)	"	49.6	47.9	51.5	"

Table 1 Simulated and observed cloud parameters and radiative fluxes for January over the Northern Hemisphere. The observed surface radiative fluxes are for winter (DJF). F,S,R refer to terrestrial, solar and total radiative fluxes, respectively.

Zonal averages

Figures 2 and 3 show a comparison of various simulated and observed radiation parameters at the top of the atmosphere (Fig.2b-d) and at the earth's surface (Fig.3) together with the cloud cover (Fig.2a). Though the cloud amount seems to be underestimated (overestimated) at low (high) latitudes, the correspondence between the simulated and observed radiation budget components is quite satisfactory: The deviations are mostly within the limits of observational error ($\pm$ 10 W/m^2). A discrepancy can be found

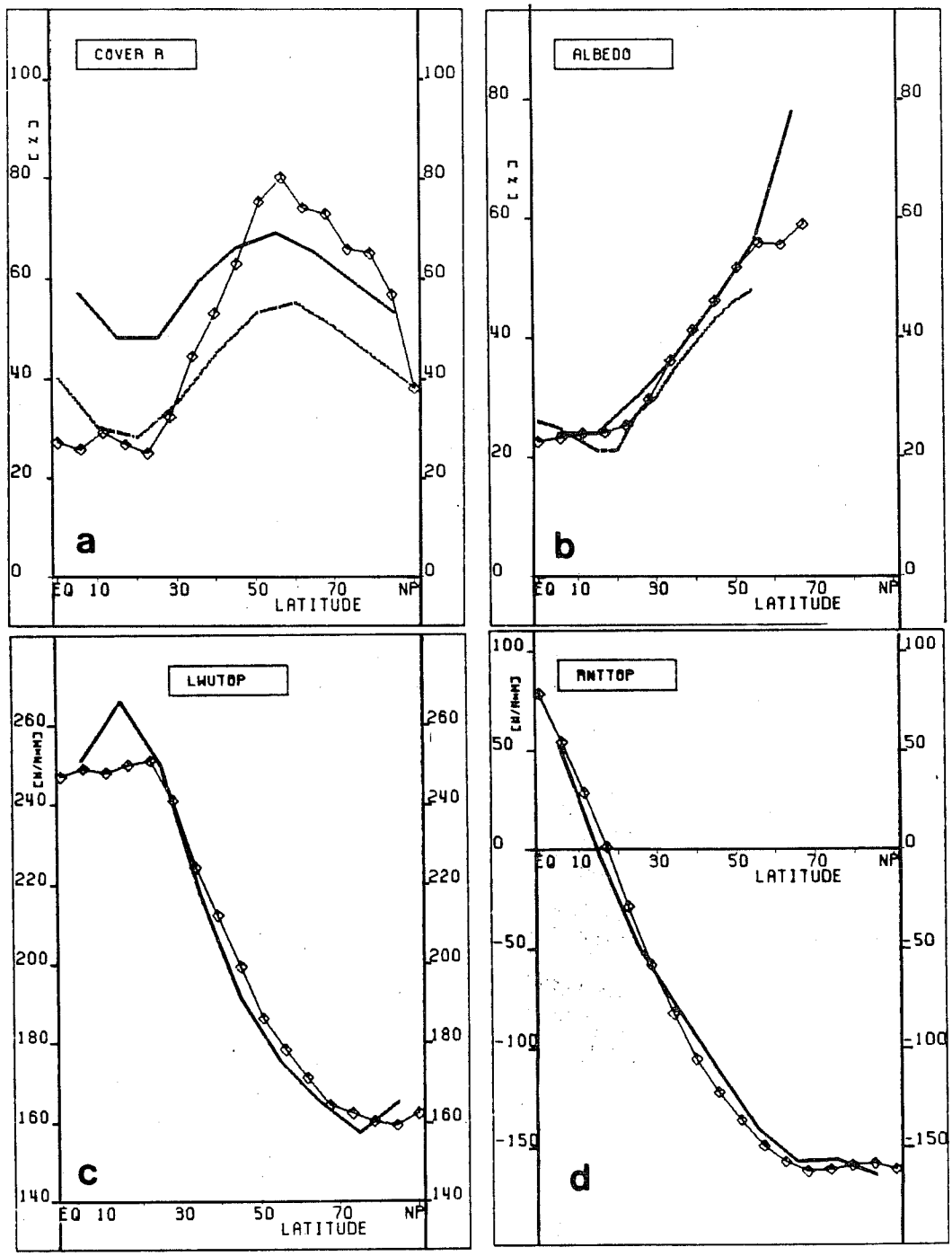

Fig.2 Latitudinal profiles of zonally averaged simulated (30d-mean) and observed cloud and radiation parameters for January. The respective simulated values are marked by symbols.

a. Total cloud cover (%). Observations are from (Solid) Berlyand and Strokina(1980) and(dashed) Hoyt (1976).

b. Albedo (%). Observations are from (solid) Stephens et al. (1981 and (dashed) Hoyt(1976).

c. Long-wave outgoing radiation at the top of the atmosphere (W/m^2). Observations (solid) are from Stephens et al.(1981).

d. As c., except for the net radiation budget.

in the tropics where the reduced outgoing longwave radiation (Fig.2c) points to large cloud amount whereas the positive deviation of the simulated net solar radiation budget at the surface (Fig.3a) indicates the opposite. An explanation can be found by looking at the vertical distribution of the simulated cloud cover (not shown): it reveals relatively large cloudiness at the upper level (20-25%) but unrealistically small cloudiness (5-10%) at the lower levels. The reason for these small values and for the large low-level cloudiness at middle and high latitudes (not shown) can be found in the choice of the same "precipitation constants" (cf.section 2.4) for "warm and "cold" clouds.

The range of observational uncertainty in cloud-cover climatologies is shown in Fig.2a where the differences between the estimates of Berlyand and Strokina(1980) and Hoyt (1976) are approximately 20% at all latitudes.

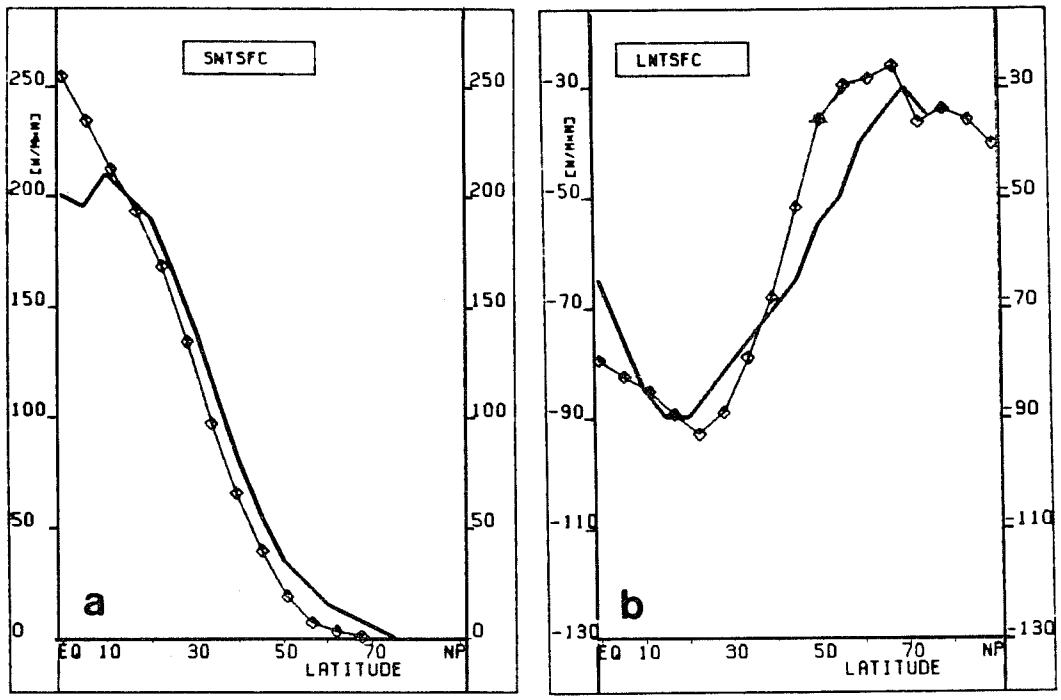

Fig.3 As fig.2c, except for

a. Net solar radiation budget at the surface.

b. Net longwave radiation budget at the surface.

Source of observations (solid): Schutz and Gates (1971).

The situation is even worse for the cloud LWC: A global LWC-climatology does not exist, so we have to rely on some recently published estimates for the period July-October 1978 (Njoku and Swanson,1983) based on satellite-derived microwave emission over the oceans south of 60°N. Fig.4 shows this observed distribution together with simulations performed with different model versions.

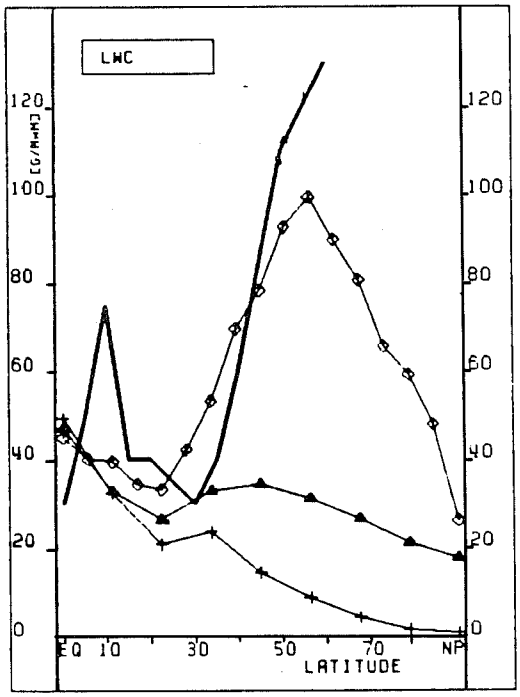

Fig. 4 As fig.2, except for total liquid water (g/m^2).

Solid: July-October 1978 (Njoku and Swanson,1983).

◇——◇ Prognostic scheme (2.8125°-grid).

▲——▲ Prognostic scheme (11.25° -grid).

+——+ Diagnostic scheme (11.25° -grid).

Apart from the observed peak at 10°N reflecting the position of the ITCZ during summer, the distribution simulated with the 2.8°-model is similar in shape to the observed one. The profiles simulated by the 11°-models deviate significantly at higher latitudes - for different reasons: In the simulation with the prognostic scheme the relatively low LWC is due to the reduced baroclinic activity in the coarse-grid model. The extremly low LWC in the simulation with the diagnostic scheme is caused by the assumption of a simple temperature dependence of LWC (Geleyn,1981), thus being independent of the model's resolution.

Hemispheric distributions

The simulated hemispheric distributions of clouds depend crucially on the simulated time-mean circulation. Fig. 5 shows the simulated 500mb geopotential height together with the simulated mean sea level pressure.

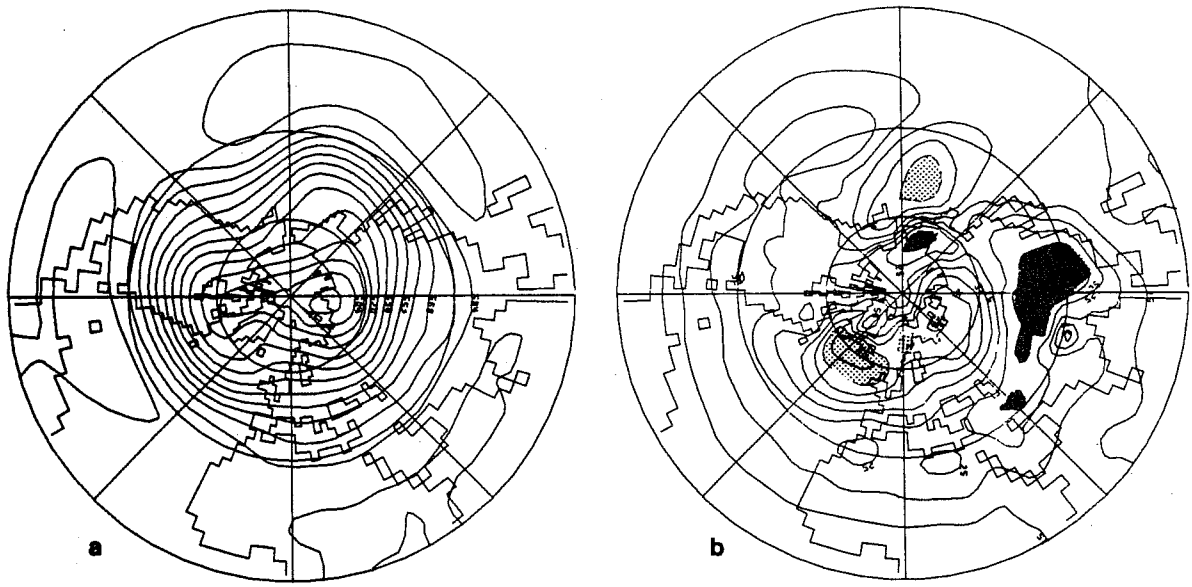

Fig.5 Simulated (30d-mean) pressure distribution over the Northern Hemisphere for January.

a. 500 mb geopotential height (spacing: 8 dam).

b. Mean sea level pressure - 1000mb (spacing: 5 mb).
Light stippling: low-pressure area (<1000 mb).
Dark " : high-" " (>1030 mb).

The main observed climatological features like the 500mb-troughs over the western parts of the midlatitude oceans and the associated Aleutian and Icelandic lows in the surface pressure field are reasonably simulated. Likewise, the divergent 500mb-flow over the western parts of the continents and the Siberian high are well represented. A feature that is generally not revealed in the observations but which can be found in many GCM-simulations is the eastward extension of the surface westerlies covering a large part of the Eurasian continent.

The simulated total cloud-cover and LWC (fig.6) is largest over the midlatitude oceans and over Eurasia. The latter maximum is certainly caused by the above mentioned overestimated cyclonic activity over Eurasia.

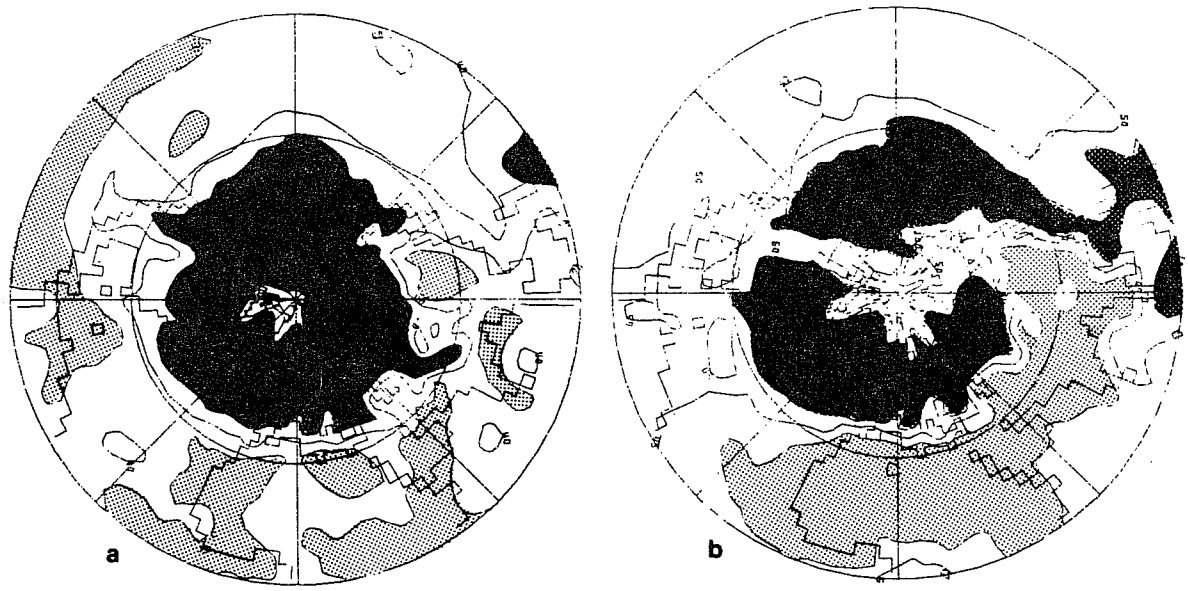

Fig.6 Simulated (30d-mean) cloud parameters over the Northern Hemisphere for January.

a. Total cloud cover CC (spacing: 20%).
Light stippling: area with CC < 20%.
Dark " : " " CC > 60%.

b. Total liquid water content LWC (spacing: 25 g/m^2).
Light stippling: area with LWC < 25 g/m^2.
Dark " : " " LWC > 75 g/m^2.

In the tropics the maxima of cloud-cover and LWC are related to the areas of large convective activity over the Western Pacific mainly and, to a lesser degree over South America. Cloud-cover of more than 20% can be found over large parts of the Sahara. However, this is exclusively due to high clouds with low LWC. On the other hand, there are areas with small total cloudiness (e.g. north of South America) but relatively large LWC produced by deep cumulus convection.

Finally, in fig.7 we show an example of the simulated longitudinal variation of outgoing longwave radiation at the top of the atmosphere (fig.7b) and its well-known dependence on high-cloud amount (fig.7a). Due to the small horizontal temperature gradients in the tropics, there exists a close correspondence between large (small) C_H-cover and small (large) outgoing longwave radiation, marked by the light and dark areas in fig.7. The minima of F(up) over the Western Pacific (200-210W/m^2) associated with a C_H-cover of more than 40%, and the maxima over Eastern Africa (270-280W/m^2) associated with a C_H-cover of less than 10% agree favourably with respective satellite observations (e.g. Gordon et al,1984).

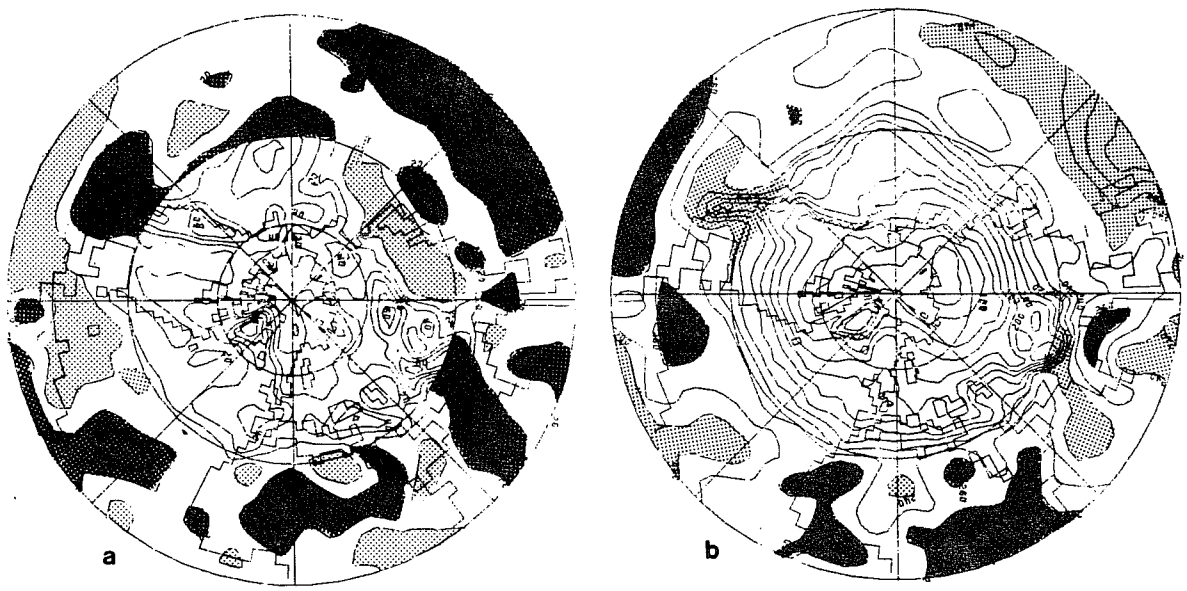

Fig.7 Simulated (30d-mean) high-cloud amount and long wave outgoing radiation at the top of the model atmosphere.

a. High-cloud amount C_H (spacing: 10%).
Light stippling: area with C_H < 10%.
Dark " : " " C_H > 20%.

b. Longwave outgoing radiation F(up) (spacing: 10 W/m^2).
Light stippling: area with F(up) < 240 W/m^2.
Dark " : " " F(up) > 260 W/m^2.

(The stippling has been done for low latitudes only.)

4. CONCLUSIONS

From a series of GCM January simulations using a prognostic cloud scheme we draw the following conclusions:

(i) With a few exceptions only, the zonally averaged earth's radiation budget is simulated within the range of observational errors.

(ii) Although a generally accepted cloud climatology does not exist, it seems fair to conclude that the simulated low-level cloudiness is underestimated at low latitudes but overestimated at high latitudes. This problem is probably related to the inadequately parameterized precipitation process which is too efficient in tropical "warm" clouds but not efficient enough in the "cold" clouds of middle and high latitudes where the "Bergeron process" is known to be important.

(iii) Advection and turbulent diffusion of cloud liquid water are negligible as compared to the microphysical terms which depend, however, crucially on the advection of water vapour and potential temperature.

(iv) One of the major advantages of the prognostic cloud scheme is that the liquid water content is calculated from the condensation rate so that the clouds are integrated into the hydrological cycle. The simulated cloud liquid water content is in reasonable agreement with the currently available (sparse) observations.

References

Berlyand, T.G. and L.A. Strokina, 1980: Global distribution of a cumulative number of clouds. Leningrad, Gidrometeoizdat.

Geleyn, J.F., 1981: Some diagnostics of the cloud/radiation interaction in ECMWF forecasting model. In ECMWF Workshop on Radiation and Cloud-Radiation Interaction in Numerical Modelling , 135-162.

Gordon, C.T., R.D. Hovanec and W.F. Stern, 1984: Analyses of monthly mean cloudiness and their influence upon model-diagnosed radiative fluxes. J. Geophys.Res., 89, 4713-4738.

Hense, A. and E. Heise, 1984: A sensitivity study of cloud parameterizations in general circulation models. Beitr. Phys. Atmosph., 57, 240-258.

Hense, A., M.Kerschgens, and E. Raschke, 1982: An economical method for computing the radiative energy transfer in circulation models. Quart. J. Roy.Meteor.Soc., 108, 231-252.

Hoyt, D.V., 1976: The radiation and energy budgets of earth using both ground based and satellite derived values of the total cloud cover. NOAA Technical Report ERL 362-ARL 4.

Kessler, E., 1969: On the distribution and continuity of water substance in atmospheric circulations.Met.Mon., 10, No.32, American Met.Soc., Boston, Mass.

Njoku, E.G. and L.Swanson, 1983: Global measurements of sea surface temperature, wind speed and atmospheric water content from satellite microwave radiometry. Mon. Wea.Rev., 111, 1977-1987.

Roeckner, E., 1979: A hemispheric model for short-range numerical weather prediction and general circulation studies. Beitr.Phys.Atmosph., 52, 262-286.

Schutz, C. and W.L. Gates, 1971: Global climatic data for surface, 800 mb, 400 mb -January.R-915-ARRP, The Rand Corporation, Santa Monica, 173 pp.

Stephens, G.L., G.G. Campbell, and T.H. Vonder Haar, 1981: Earth radiation budgets. J. Geophys. Res., 86, 9739-9760.

Sundqvist, H., 1978: A parameterization scheme for non-convective condensation including prediction of cloud water content. Quart. J. Roy. Meteor.Soc., 104, 677-690.